A Zener model for nonlinear viscoelastic waves

N Favrie, Bruno Lombard

A Zener model for nonlinear viscoelastic waves

N. Favrie and B. Lombard

June 27, 2022

Abstract

A macroscopic model describing nonlinear viscoelastic waves is derived in Eulerian formulation, through the introduction of relaxation tensors. In the limiting case of small deformations, the governing equations recover those of the linear Zener model with memory variables, which is widely used in acoustics. The structure of the relaxation terms ensures that the model is dissipative. The chosen family of specific internal energies ensures also that the model is unconditionally hyperbolic. Numerical examples are proposed to illustrate the properties of viscoelastic waves, in small and large deformations.

Keywords: Hyperelasticity, Zener model, memory variables, hyperbolic systems

1 Introduction

Wave motion in real media differs in many aspects from motion in an idealized elastic medium. The dispersion and attenuation induced, for instance, by grain-to-grain friction can greatly affect the amplitude of the waves and their arrival times.

Usually, linear viscoelasticity is assumed to provide reasonably accurate means of describing these effects. Viscoelastic constitutive laws give the stress in terms of the past strain rate history. Among the many existing models, the linear Zener's model has proven its ability to describe the viscoelastic behaviour in small deformation of various type of materials [5]. It accounts for quite general attenuation laws, such as quality factors with a frequency power law. Introduction of memory variables yields a hyperbolic local-in-time evolution problem, which is computationally affordable [28, 21].

However, the linear framework is insufficient to describe wave propagation in many interesting configurations. In the biomedical context, both nonlinearities and viscoelasticity are needed to model shock waves in soft solids such as the brain or the liver [8, 29]. In granular media, the physical source of the nonlinearities and attenuation is associated to grain-to-grain interactions [31]. At a larger scale, nonlinearities and viscous damping arising during the wave propagation are commonly studied in the context of site effect assessment, and related resonance phenomena [7]. In the acoustical litterature, nonlinear mechanisms are generally introduced heuristically into existing linear models. For example, a nonlinear term has been added to the linear Zener model [22], but within the framework of a linear constitutive law and infinitesimal strains. Such a methodology raises two fundamental questions: (i) are the underlying approximations consistent? (ii) what are their mathematical and physical properties of the resulting equations?

A rational answer to these questions can be found by turning to the literature of solid mechanics. Numerous works have focused on the coupling of viscoelasticity and hyperelastic behavior laws

in finite strain. The reader is referred to reference works such as [17, 19, 32] for an overview of the dedicated litterature. Nevertheless, these models are often designed in the quasi-static regime, and they do not incorporate the particularities of wave phenomena. In particular, viscoelastic models for nonlinear waves should ensure a finite propagation speed, leading to explicit-in-time numerical schemes. Finally, the model parameters should be identifiable from classical acoustic measurements (phase velocity, quality factor).

In summary, the construction of nonlinear viscoelastic models for wave propagation needs to incorporate both the rigor of rational mechanics and the specificities of wave propagation. The criteria of choice that we consider the most important are: (i) to be thermodynamically consistent; (ii) to yield a well-posed initial-valued problem that is local in time; (iii) to degenerate towards the linear Zener model in the limit-case of small deformations. The objective of this paper is to propose such a consistent model. An approach satisfying (i)-(ii) has been proposed in [18], in the incompressible case. The present work can be seen as an extension of this paper to the compressible case, with additionally the criterion (iii) unconditionnaly satisfied. On the other hand, a Zener model satisfying the three criteria has already been developed by the authors, but in the one-dimensional case [13, 2]. One aim of the present article is to generalize these 1D works to higher spatial dimensions, in a rigorous tensorial framework.

For this purpose, our approach is based on hyperelasticity where relaxation tensors are introduced. The model is built in an Eulerian framework and yields a nonlinear hyperbolic set of first-order partial differential equations with source terms (a Lagrangian formulation would require only small adjustments). One parameter of the model controls the nonlinearity. On a bounded interval of values, this parameter ensures hyperbolicity of the governing equations [24, 15]. The other parameters can be calibrated in the linear regime, based on an optimization procedure described in [3]. The numerical solution can be estimated based on a splitting method: the hyperbolic part is solved by a Godunov-type HLLC scheme, while the relaxation part is solved analytically.

The paper is organised as follows. In Section 2, we present the linear Zener model and the hyperelastic model in Eulerian formulation. The nonlinear Zener model is introduced in Section 3, together with the equation of state and a way to calibrate the parameters. A numerical scheme is proposed in Section 4. Numerical experiments illustrate the wave phenomena in Section 5, for various magnitudes of nonlinearity. Conclusion is drawn in Section 6.

2 Limit cases

2.1 Linear viscoelasticity

The linear Zener model is largely used in acoustics and in computational seismology. This model adequately describes the usual relaxation and creep tests of solids under small deformations [5]. By optimizing its parameters, the Zener model allows to finely describe dispersion relations of the waves [3]. The relaxation functions of compressional (P) and shear (S) waves write respectively

$$\psi_\pi(t) = \pi_r \left(1 + \sum_{\ell=1}^{N} \kappa_\ell^p \, e^{-\theta_\ell t}\right) H(t), \qquad \psi_\mu(t) = \mu_r \left(1 + \sum_{\ell=1}^{N} \kappa_\ell^s \, e^{-\theta_\ell t}\right) H(t), \tag{1}$$

where H is the Heaviside function, N is the number of relaxation mechanisms, θ_ℓ are relaxation frequencies, and the parameters $\kappa_\ell^{p,s}$ are positive weights. Describing P and S waves with identical relaxation frequencies, as well as identical numbers of relaxation mechanisms, allows to greatly

reduce the memory requirements [28]. In (1), $\pi_r = \rho\, c_p^2(0)$ and $\mu_r = \rho\, c_s^2(0)$ are relaxed moduli under compressional and shear loads, where $c_p(0)$ and $c_s(0)$ denote the phase velocities of P and S waves at zero frequency, respectively. The unrelaxed moduli are

$$\pi_u = \pi_r \left(1 + \sum_{\ell=1}^{N} \kappa_\ell^p\right) = \rho_0\, c_p^2(\infty), \qquad \mu_u = \mu_r \left(1 + \sum_{\ell=1}^{N} \kappa_\ell^s\right) = \rho_0\, c_s^2(\infty), \tag{2}$$

where $c_p(\infty)$ and $c_s(\infty)$ are the phase velocities of P and S waves at infinite frequency, and ρ_0 is a reference density.

A naive use of the relaxation functions (1) would involve convolution products, which is computationally too expensive. Introducing the so-called *memory variables* ξ_ℓ provides a local-in-time hyperbolic system with source term. The velocity-stress formulation writes [21]:

$$\begin{cases} \rho_0 \dfrac{\partial \mathbf{v}}{\partial t} = \operatorname{div}(\sigma), & \text{(3a)} \\ \dfrac{\partial \sigma}{\partial t} = (\pi_u - 2\,\mu_u) \operatorname{div}(\mathbf{v})\, \mathbf{I} + 2\,\mu_u \mathbf{D} + \displaystyle\sum_{\ell=1}^{N} \xi_\ell, & \text{(3b)} \\ \dfrac{\partial \xi_\ell}{\partial t} = -\theta_\ell \left((\pi_r \kappa_\ell^p - 2\mu_r \kappa_\ell^s) \operatorname{div}(\mathbf{v})\, \mathbf{I} + 2\mu_r \kappa_\ell^s\, \mathbf{D} + \xi_\ell \right), \qquad \ell = 1, \cdots, N, & \text{(3c)} \end{cases}$$

where $\mathbf{v} = (u, v, w)^T$ is the velocity, σ is the Cauchy stress, and ξ_ℓ are symmetric tensors.

2.2 Nonlinear hyperelasticity

The conservation of mass, momentum and energy in Eulerian formulation writes:

$$\begin{cases} \dfrac{\partial \rho}{\partial t} + \operatorname{div}(\rho \mathbf{v}) = 0, & \text{(4a)} \\ \dfrac{\partial (\rho \mathbf{v})}{\partial t} + \operatorname{div}(\rho \mathbf{v} \otimes \mathbf{v} - \sigma) = \mathbf{0}, & \text{(4b)} \\ \dfrac{\partial (\rho E)}{\partial t} + \operatorname{div}(\rho \mathbf{v} E - \sigma \mathbf{v}) = 0, & \text{(4c)} \end{cases}$$

and the kinematic equation is

$$\frac{d}{dt} \mathbf{F}^{-\top} = -\mathbf{grad}^{\top}(\mathbf{v}).\, \mathbf{F}^{-\top}. \tag{5}$$

The system (4)-(5) yields 7 waves [16]. The differential operators are applied in the Eulerian coordinates $\mathbf{x} = (x, y, z)^{\top} \in \mathbb{R}^3$. The deformation gradient is $\mathbf{F}$. The density is $\rho = \rho_0 / |\mathbf{F}|$, where ρ_0 is a reference density and $|\bullet| = \det(\bullet)$. The total specific energy E is

$$E = \frac{\mathbf{v}^2}{2} + e(\eta, \mathbf{C}^{-1}), \tag{6}$$

where e is the specific internal energy, η is the specific entropy, and $\mathbf{C} = \mathbf{F}^T.\mathbf{F}$ is the right Cauchy-Green strain tensor. The nullity of dissipation yields the Cauchy stress tensor:

$$\sigma = -2\,\rho\, \mathbf{F}^{-\top}. \frac{\partial e}{\partial \mathbf{C}^{-1}}. \mathbf{F}^{-1}. \tag{7}$$

Using $\mathbf{C}^{-1}$ in (6) ensures the symmetry of σ even in the anisotropic case.

3 Nonlinear Zener model

3.1 Objective

We aim to build a model that satisfies the following properties:

(i) recovering the linear Zener model (3) in the case of infinitesimal deformation;

(ii) recovering the hyperelastic model (4) in the lossless case;

(iii) satisfying the second principle of thermodynamics;

(iv) being unconditionally hyperbolic.

This new model is built by adding to the system (4) relaxation terms (Section 3-3.2). The study of this model in small deformations in Section 3-3.3 leads, by identifying the parameters, to the linear Zener model (criterion (i)). When these terms cancel, the hyperelastic model is recovered, which satisfies criterion (ii). The general form of the relaxation terms is determined by imposing a positive dissipation, thus satisfying criterion (iii). Finally, criterion (iv) is satisfied by choosing particular forms of specific internal energy (Section 3-3.4).

3.2 Governing equations

The conservation equations (4) are unchanged. However, we introduce new kinematic variables denoted $\mathbf{F}_\ell$. These variable can be seen as the elastic part in the multiplicative decomposition if only one mechanism is considered. Thus, the kinematic equations (5) reads:

$$\begin{cases} \dfrac{d}{dt}\mathbf{F}_0^{-\top} = -\mathbf{grad}^\top(\mathbf{v}).\,\mathbf{F}_0^{-\top}, & \text{(8a)} \\ \dfrac{d}{dt}\mathbf{F}_\ell^{-\top} = -\mathbf{grad}^\top(\mathbf{v}).\,\mathbf{F}_\ell^{-\top} + \mathbf{R}_\ell.\,\mathbf{F}_\ell^{-\top}, \qquad \ell = 1, \cdots, N. & \text{(8b)} \end{cases}$$

Here $\mathbf{R}_\ell$ are symmetric second-order tensors. These relaxation terms will be determined later. A similar approach is used to model viscoplasticity in [9] or incompressible viscoelasticity in [18, 27]. Equation (8a) describes the elastic part of the behaviour. It can be merged with (8b) by setting $\mathbf{R}_0 = \mathbf{0}$, as done from now. Based on (8b), the time derivative of $\mathbf{C}_\ell^{-1} = \mathbf{F}_\ell^{-1}.\,\mathbf{F}_\ell^{-\top}$ writes:

$$\frac{d}{dt}\mathbf{C}_\ell^{-1} = -2\,\mathbf{F}_\ell^{-1}.\,\mathbf{D}.\,\mathbf{F}_\ell^{-\top} + 2\,\mathbf{F}_\ell^{-1}.\,\mathbf{R}_\ell.\,\mathbf{F}_\ell^{-\top}, \qquad \ell = 1, \cdots, N, \tag{9}$$

where $\mathbf{D} = \mathrm{sym}(\mathbf{grad}(\mathbf{v}))$ is the strain rate.

Dissipation of energy. The total specific energy is

$$E = \frac{\mathbf{v}^2}{2} + \sum_0 e_\ell\left(\eta, \mathbf{C}_\ell^{-1}\right). \tag{10}$$

The Cauchy stress

$$\sigma = \sum_{\ell=0}^{N} \sigma_\ell \tag{11}$$

is deduced from the Gibbs identity and the second principle of thermodynamics: using (9), (10) and the symmetry of $\mathbf{D}$ and $\mathbf{R}_\ell$, the dissipation $\mathcal{D}$ writes

$$\begin{aligned}
\mathcal{D} &= \sum_{\ell=0}^{N} \left(\sigma_\ell : \mathbf{D} - \rho \frac{\partial e_\ell}{\partial \mathbf{C}_\ell^{-1}} : \frac{d}{dt}\mathbf{C}_\ell^{-1} \right), \\
&= \sum_{\ell=0}^{N} \left(\sigma_\ell : \mathbf{D} - \rho \frac{\partial e_\ell}{\partial \mathbf{C}_\ell^{-1}} : \left(-2\,\mathbf{F}_\ell^{-1}.\mathbf{D}.\mathbf{F}_\ell^{-\top} + 2\,\mathbf{F}_\ell^{-1}.\mathbf{R}_\ell.\mathbf{F}_\ell^{-\top} \right) \right), \\
&= \sum_{\ell=0}^{N} \left(\left(\sigma_\ell + 2\,\rho\,\mathbf{F}_\ell^{-\top}.\frac{\partial e_\ell}{\partial \mathbf{C}_\ell^{-1}}.\mathbf{F}_\ell^{-1} \right) : \mathbf{D} - 2\,\rho\,\mathbf{F}_\ell^{-\top}.\frac{\partial e_\ell}{\partial \mathbf{C}_\ell^{-1}}.\mathbf{F}_\ell^{-1} : \mathbf{R}_\ell \right), \\
&\geq 0.
\end{aligned} \tag{12}$$

This inequality is satisfied whatever $\mathbf{D}$, which implies

$$\sigma_\ell = -2\,\rho\,\mathbf{F}_\ell^{-\top}.\frac{\partial e_\ell}{\partial \mathbf{C}_\ell^{-1}}.\mathbf{F}_\ell^{-1}, \qquad \ell = 0, \cdots, N, \tag{13}$$

and

$$\sum_{\ell=0}^{N} \sigma_\ell : \mathbf{R}_\ell = \sum_{\ell=0}^{N} \mathrm{tr}\left(\sigma_\ell.\mathbf{R}_\ell\right) \geq 0. \tag{14}$$

Property 1 *A sufficient condition to ensure* (14) *is to choose:*

$$\mathbf{R}_\ell = \alpha_\ell\,\sigma_\ell + \beta_\ell\,tr(\sigma_\ell)\,\mathbf{I}, \qquad \ell = 1, \cdots, N, \tag{15}$$

where $\mathbf{I}$ *is the second-order identity tensor,* $\alpha_\ell \geq 0$ *and* $\beta_\ell \geq -\alpha_\ell/3$.

The parameters α_ℓ and β_ℓ are scalar and may depend on any parameters such as temperature, invariant of the stress, pressure, etc. In the following and for the sake of simplicity, we will consider them as constant. **Proof.** The tensor σ_ℓ is split into its spheric and deviatoric parts:

$$\sigma_\ell = -p_\ell\,\mathbf{I} + \mathbf{S}_\ell, \text{ with } \mathrm{tr}(\mathbf{S}_\ell) = 0. \tag{16}$$

Then one has:

$$\begin{aligned}
\mathrm{tr}\left(\sigma_\ell.\mathbf{R}_\ell\right) &= \mathrm{tr}\left(\left(-p_\ell\,\mathbf{I} + \mathbf{S}_\ell\right) \left(\alpha_\ell(-p_\ell\,\mathbf{I} + \mathbf{S}_\ell) + \beta_\ell(-3\,p_\ell)\,\mathbf{I}\right) \right), \\
&= \left(\alpha_\ell + 3\,\beta_\ell\right)\,p_\ell^2\,\mathrm{tr}(\mathbf{I}) - \left(2\,\alpha_\ell + 3\,\beta_\ell\right)\,p_\ell\,\mathrm{tr}(\mathbf{S}_\ell) + \alpha_\ell\,\mathrm{tr}(\mathbf{S}_\ell^2), \\
&= 3\left(\alpha_\ell + 3\,\beta_\ell\right)\,p_\ell^2 + \alpha_\ell\,\mathbf{S}_\ell : \mathbf{S}_\ell, \\
&\geq 0,
\end{aligned} \tag{17}$$

which concludes the proof. ■

Property 1 generalizes the analysis performed in [9] in the case of viscoplasticity. The determination of α_ℓ and β_ℓ will be discussed in Section 3.3 to guaranty that, in the limit of small deformation, the model recovers the generalized Zener model used in acoustics.

Evolution of $|\mathbf{F}_\ell|$. For further calibration of the equation of state and numerical resolution of the governing equations, the time derivative of $J_\ell = |\mathbf{C}_\ell| = |\mathbf{F}_\ell|^2$ is needed. Based on (9), it follows that:

$$\frac{d}{dt}J_\ell = 2J_\ell\left(\mathrm{div}(\mathbf{v}) - \mathrm{tr}(\mathbf{R}_\ell)\right), \qquad \ell = 1, \cdots, N. \tag{18}$$

Using (18) and $J_\ell^{-1} = (J_\ell^{-1/2})^2$, one obtains

$$\frac{d}{dt}J_\ell^{-1/2} + J_\ell^{-1/2}\mathrm{div}(\mathbf{v}) = J_\ell^{-1/2}\mathrm{tr}(\mathbf{R}_\ell), \qquad \ell = 1, \cdots, N. \tag{19}$$

3.3 Small deformations

In the case of small deformations, the Lagrangian and Eulerian descriptions are identical and $\mathbf{C}_\ell^{-1} \approx \mathbf{I} - 2\,\varepsilon_\ell$, where ε_ℓ are second-order symmetric tensors. Using (9) leads to

$$\frac{\partial \varepsilon_\ell}{\partial t} = \mathbf{D} - \mathbf{R}_\ell, \qquad \ell = 1, \cdots, N. \tag{20}$$

The constitutive laws for linear isotropic solids write $\sigma_\ell = \lambda_\ell \,\mathrm{tr}(\varepsilon_\ell)\,\mathbf{I} + 2\,\mu_\ell\,\varepsilon_\ell$, where λ_ℓ and μ_ℓ are Lamé coefficients, to be determined. Time differentiating the constitutive laws and using (20) gives

$$\frac{\partial \sigma_\ell}{\partial t} = \lambda_\ell \,\mathrm{div}(\mathbf{v})\,\mathbf{I} + 2\,\mu_\ell\,\mathbf{D} + \xi_\ell, \qquad \ell = 1, \cdots, N, \tag{21}$$

where the second-order symmetric tensors ξ_ℓ write

$$\xi_\ell = -\left(\lambda_\ell \,\mathrm{tr}(\mathbf{R}_\ell)\,\mathbf{I} + 2\,\mu_\ell\,\mathbf{R}_\ell\right), \qquad \ell = 1, \cdots, N, \tag{22}$$

and $\xi_0 = \mathbf{0}$. Introducing the unrelaxed moduli

$$\pi_u = \sum_{\ell=0}^{N} \left(\lambda_\ell + 2\,\mu_\ell\right), \qquad \mu_u = \sum_{\ell=0}^{N} \mu_\ell, \tag{23}$$

and summing (21) over ℓ, one obtains

$$\frac{\partial \sigma}{\partial t} = \left(\pi_u - 2\,\mu_u\right) \mathrm{div}(\mathbf{v})\,\mathbf{I} + 2\,\mu_u \mathbf{D} + \sum_{\ell=1}^{N} \xi_\ell, \tag{24}$$

which recovers the evolution of σ in the linear Zener model (3b). It remains to determine the time evolution of ξ_ℓ. From (21), it follows

$$\frac{\partial}{\partial t}\mathrm{tr}(\sigma_\ell) = (3\lambda_\ell + 2\mu_\ell)\ \mathrm{div}(\mathbf{v}) + \mathrm{tr}(\xi_\ell), \qquad \ell = 1, \cdots, N. \tag{25}$$

Equations (15) and (22) yield

$$\xi_\ell = -\left(A_\ell\,\sigma_\ell + B_\ell \,\mathrm{tr}(\sigma_\ell)\,\mathbf{I}\right), \qquad \ell = 1, \cdots, N, \tag{26}$$

with

$$A_\ell = 2\,\mu_\ell\,\alpha_\ell, \qquad B_\ell = \lambda_\ell\,\alpha_\ell + (3\lambda_\ell + 2\,\mu_\ell)\ \beta_\ell, \qquad \ell = 1, \cdots, N. \tag{27}$$

From (21), (25) and (26), one deduces

$$\frac{\partial \xi_\ell}{\partial t} = -A_\ell\left(\lambda_\ell \,\mathrm{div}(\mathbf{v})\,\mathbf{I} + 2\,\mu_\ell\,\mathbf{D} + \xi_\ell\right) - B_\ell\left((3\lambda_\ell + 2\mu_\ell)\ \mathrm{div}(\mathbf{v}) + \mathrm{tr}(\xi_\ell)\right)\mathbf{I}, \qquad \ell = 1, \cdots, N. \tag{28}$$

Identification with (3c), where no term $\mathrm{tr}(\xi_\ell)$ occurs, implies $B_\ell = 0$, and (27) gives

$$\beta_\ell = -\frac{\lambda_\ell}{3\lambda_\ell + 2\mu_\ell}\,\alpha_\ell, \qquad \ell = 1, \cdots, N. \tag{29}$$

The equation (28) then recovers the evolution of ξ_ℓ in the linear Zener model (3c) if the following conditions are satisfied ($\ell = 1, \cdots, N$):

$$\lambda_\ell = \pi_r \kappa_\ell^p - 2\mu_r \kappa_\ell^s, \qquad \mu_\ell = \mu_r \kappa_\ell^s, \qquad \alpha_\ell = \frac{\theta_\ell}{2\mu_\ell} = \frac{\theta_\ell}{2\mu_r \kappa_\ell^s}. \tag{30}$$

The parameters of the linear Zener model κ_ℓ^p, κ_ℓ^s and θ_ℓ can be obtained from the attenuation of linear P and S waves [3]. The elastic moduli λ_0 and μ_0 are determined by using (23):

$$\lambda_0 = \pi_u - \mu_u - \sum_{\ell=1}^{N} \lambda_\ell, \qquad \mu_0 = \mu_u - \sum_{\ell=1}^{N} \mu_\ell. \tag{31}$$

3.4 Equations of state

One considers materials with a specific internal energy (10) in separable form:

$$e_\ell(\eta, \mathbf{C}_\ell^{-1}) = e_\ell^h(J_\ell) + e_\ell^e(\hat{\mathbf{C}}_\ell^{-1}), \qquad \ell = 1, \cdots, N, \tag{32}$$

with the unimodular tensor $\hat{\mathbf{C}}_\ell^{-1} = \mathbf{C}_\ell^{-1} / \left|\mathbf{C}_\ell^{-1}\right|^{1/3}$. The hydrodynamic part of the energy e_ℓ^h depends only on the volume change, whereas the shear part of the energy e_ℓ^e is unaffected by the volume change. For isotropic solids, e_ℓ^e can be written as a function of only two invariants of $\hat{\mathbf{C}}_\ell^{-1}$:

$$e_\ell^e(\hat{\mathbf{C}}_\ell^{-1}) = e_\ell^e(j_{1\ell}, j_{2\ell}), \qquad j_{k\ell} = \mathrm{tr}\left(\left(\hat{\mathbf{C}}_\ell^{-1}\right)^k\right) \equiv \mathrm{tr}\left(\left(\hat{\mathbf{G}}_\ell\right)^k\right), \tag{33}$$

with the unimodular parts of the Finger tensors $\hat{\mathbf{G}}_\ell = \mathbf{G}_\ell / \left|\mathbf{G}_\ell\right|^{1/3}$, where $\mathbf{G}_\ell = \mathbf{B}_\ell^{-1}$ is the Finger tensor and $\mathbf{B}_\ell = \mathbf{F}_\ell . \mathbf{F}_\ell^T$ is the left Cauchy-Green deformation tensor. Based on the usual relations of tensorial calculus

$$\frac{\partial}{\partial \mathbf{A}} \mathrm{tr}\left(\mathbf{A}^n\right) = n \left(\mathbf{A}^T\right)^{n-1}, \qquad \frac{\partial}{\partial \mathbf{A}} \det(\mathbf{A}) = \det(\mathbf{A})\, \mathbf{A}^{-\top}, \tag{34}$$

the Cauchy stress in (13) writes ($\ell = 1, \cdots, N$):

$$\begin{aligned}
\sigma_\ell &= -2\,\rho\, \mathbf{F}_\ell^{-\top} \left(\frac{\partial e_\ell^h}{\partial J_\ell} \frac{\partial J_\ell}{\partial \mathbf{C}_\ell^{-1}} + \sum_{k=1}^{2} \frac{\partial e_\ell^e}{\partial j_{k\ell}} \frac{\partial j_{k\ell}}{\partial \mathbf{C}_\ell^{-1}} \right) . \mathbf{F}_\ell^{-1}, \\
&= -2\,\rho\, \mathbf{F}_\ell^{-\top} \left(-\frac{\partial e_\ell^h}{\partial J_\ell} J_\ell\, \mathbf{C}_\ell + \sum_{k=1}^{2} \frac{\partial e_\ell^e}{\partial j_{k\ell}} k \left(J_\ell^{k/3} \left(\mathbf{C}_\ell^{-1}\right)^k - \frac{j_{k\ell}}{3}\, \mathbf{I} \right) \mathbf{C}_\ell \right) . \mathbf{F}_\ell^{-1}, \\
&\equiv -p_\ell\, \mathbf{I} + \mathbf{S}_\ell,
\end{aligned} \tag{35}$$

with $\mathrm{tr}(\mathbf{S}_\ell) = 0$. The hydrodynamic part of the stress is thus

$$p_\ell = -2\rho \frac{\partial e_\ell^h}{\partial J_\ell} J_\ell, \tag{36}$$

whereas the deviatoric part of the stress writes

$$\begin{aligned}
\mathbf{S}_\ell &= -2\rho \left(\frac{\partial e_\ell^e}{\partial j_{1\ell}} \left(J_\ell^{1/3} \mathbf{F}_\ell^{-\top} . \mathbf{F}_\ell^{-1} - \frac{j_{1\ell}}{3}\, \mathbf{I} \right) + 2 \frac{\partial e_\ell^e}{\partial j_{2\ell}} \left(J_\ell^{2/3} \left(\mathbf{F}_\ell^{-\top} . \mathbf{F}_\ell^{-1}\right)^2 - \frac{j_{2\ell}}{3}\, \mathbf{I} \right) \right), \\
&= -2\rho \left(\frac{\partial e_\ell^e}{\partial j_{1\ell}} \left(\hat{\mathbf{G}}_\ell - \frac{j_{1\ell}}{3}\, \mathbf{I} \right) + 2 \frac{\partial e_\ell^e}{\partial j_{2\ell}} \left(\left(\hat{\mathbf{G}}_\ell\right)^2 - \frac{j_{2\ell}}{3}\, \mathbf{I} \right) \right).
\end{aligned} \tag{37}$$

The last expression in (37) recovers the shear tensor given in [12, 15]: in the isotropic case, the stress equations deduced from the Finger tensors and from $\mathbf{C}_\ell^{-1}$ are thus the same. Now we determine the stresses induced by the internal energy (32).

Hydrodynamic stress. The hydrodynamic part of the energy is chosen in the form:

$$e_\ell^h(\eta, J_\ell) = \frac{d_\ell}{\rho_0} \left(J_\ell^{1/2} - 1 \right)^2, \qquad \ell = 0, \cdots, N, \tag{38}$$

where ρ_0 is a reference density. This convex energy ensures hyperbolicity of (8) in the absence of shear energy. Using (36) and $\rho = \rho_0 / J_0^{1/2}$ yields the pressures

$$p_\ell = 2\, d_\ell \frac{\rho}{\rho_0} J_\ell^{1/2} \left(1 - J_\ell^{1/2} \right) = 2\, d_\ell \left(\frac{J_\ell}{J_0} \right)^{1/2} \left(1 - J_\ell^{1/2} \right). \tag{39}$$

The hydrodynamic sound velocities are

$$c_{h\ell}^2 = 2\,J_\ell \left(\frac{\partial e_\ell^h}{\partial J_\ell} + 2J_\ell \frac{\partial^2 e_\ell^h}{\partial J_\ell^2} \right) = \frac{2d_\ell}{\rho_0} J_\ell, \qquad \ell = 0, \cdots, N. \tag{40}$$

The inequality $J_\ell > 0$ must always be satisfied to yield real hydrodynamic sound velocities. The nonlinear parameter d_ℓ is determined in two steps, based on the limit-case of small deformations. First, in the isentropic case, the differential of $p_\ell(\eta, \rho, J_\ell)$ writes

$$\frac{dp_\ell}{dt} = \frac{dp_\ell}{d\rho}\frac{d\rho}{dt} + \frac{dp_\ell}{dJ_\ell}\frac{dJ_\ell}{dt}. \tag{41}$$

The latter is deployed based on (36), on the conservation of mass (4a) and on the transport of J_ℓ (18), leading to

$$\frac{dp_\ell}{dt} = -2\rho\, J_\ell \left(\frac{\partial e_\ell^h}{\partial J_\ell} + 2J_\ell \frac{\partial^2 e_\ell^h}{\partial J_\ell^2} \right) \mathrm{div}(\mathbf{v}) + 4\rho\, J_\ell \left(\frac{\partial e_\ell^h}{\partial J_\ell} + 2J_\ell \frac{\partial^2 e_\ell^h}{\partial J_\ell^2} \right) \mathrm{tr}(\mathbf{R}_\ell). \tag{42}$$

Second, the decomposition (16) leads to $p_\ell = -1/3\,\mathrm{tr}(\sigma_\ell)$, which is then time differentiated in the case of small deformations (25):

$$\frac{dp_\ell}{dt} \approx \frac{\partial p_\ell}{\partial t} = -\left(\lambda_\ell + \frac{2}{3}\mu_\ell\right) \mathrm{div}(\mathbf{v}) - \frac{1}{3}\mathrm{tr}(\xi_\ell). \tag{43}$$

Identification between (42) and (43) gives

$$2\rho\, J_\ell \left(\frac{\partial e_\ell^h}{\partial J_\ell} + 2\, J_\ell \frac{\partial^2 e_\ell^h}{\partial J_\ell^2} \right) = \lambda_\ell + \frac{2}{3}\mu_\ell. \tag{44}$$

The left hand side of (44) is deduced from the hydrodynamic energy (38) and equals $2(\rho/\rho_0) J_\ell\, d_\ell$. For small deformations, $\rho \approx \rho_0$ and $J_\ell \approx 1$. Using (44) yields the nonlinear parameter

$$d_\ell = \frac{1}{2}\left(\lambda_\ell + \frac{2}{3}\mu_\ell\right), \qquad \ell = 0, \cdots, N. \tag{45}$$

Deviatoric stress. The shear part of the energy (33) is chosen in the form [12]:

$$e_\ell^e(j_{1\ell}, j_{2\ell}) = \frac{\mu_\ell}{4\rho_0}\left(\chi_\ell\, j_{2\ell} + \frac{1-2\chi_\ell}{3}\, j_{1\ell}^2 + 3\,(\chi_\ell - 1) \right), \qquad \ell = 0, \cdots, N. \tag{46}$$

Here χ_ℓ can be viewed as new nonlinear parameters. For small deformations and any χ_ℓ, the Hooke law is recovered. Thus, these parameters are important only in the case of large shear deformations. They can be used to fit experimental data. The deviatoric part of the stress is finally deduced from (37) and (46), through

$$\frac{\partial e_\ell^e}{\partial j_{1\ell}} = \frac{\mu_\ell}{6\,\rho_0}\,(1-2\chi_\ell)\, j_{1\ell}, \qquad \frac{\partial e_\ell^e}{\partial j_{2\ell}} = \frac{\mu_\ell}{4\,\rho_0}\chi_\ell, \qquad \ell = 0, \cdots, N. \tag{47}$$

A theoretical analysis of (46) has been performed in hyperelasticity [15]. The unconditional hyperbolicity was proven under the sufficient condition $-1 \leq \chi \leq 0.5$. With such a choice for each χ_ℓ and following [24], one can prove that the nonlinear Zener model model is also hyperbolic in the whole range of solutions. The limit case $\chi_\ell = -1$ corresponds to Neo-Hookean solids. Other choices of equations of state are of course possible, for example the Mooney-Rivlin model often used for elastomers, or the Murnaghan model widely used for non-destructive testing of geomaterials [1]. However, hyperbolicity has not been proven for these models.

3.5 Final system

The governing equations of the nonlinear Zener model are summarized in the following system of $14 + 10 \times N$ partial differential equations:

$$\begin{cases} \dfrac{\partial \rho}{\partial t} + \mathrm{div}(\rho \mathbf{v}) = 0, & \text{(48a)} \\ \dfrac{\partial (\rho \mathbf{v})}{\partial t} + \mathrm{div}(\rho \mathbf{v} \otimes \mathbf{v} - \sigma) = \mathbf{s}, & \text{(48b)} \\ \dfrac{\partial \mathbf{e}_\ell^\beta}{\partial t} + \mathbf{grad}(\mathbf{e}_\ell^\beta).\mathbf{v} + \mathbf{e}_\ell^\beta.\mathbf{grad}(\mathbf{v}) = \mathbf{R}_\ell.\mathbf{e}_\ell^\beta, \qquad \ell = 0, \cdots, N, \qquad \beta = 1,2,3, & \text{(48c)} \\ \dfrac{\partial}{\partial t} J_\ell^{-1/2} + \mathrm{div}\left(J_\ell^{-1/2} \mathbf{v} \right) = \phi_\ell, \qquad \ell = 0, \cdots, N. & \text{(48d)} \end{cases}$$

In (48b), $\mathbf{s}$ is a bulk force term. The system (48) needs to be completed by initial conditions. In the case of forcing by a source point $\mathbf{s} \neq \mathbf{0}$, then the initial data are $\rho(\bullet, t = 0) = \rho_0$, $\mathbf{v}(\bullet, t = 0) = \mathbf{0}$, $\mathbf{F}_\ell^{-\top}(\bullet, t = 0) = \mathbf{I}$ and $J_\ell^{-1/2}(\bullet, t = 0) = 1$.

The conservation of energy (4c) is not recalled, since the internal energy does not depend on entropy. The components of the Cauchy stress σ (11)-(35) are the hydrodynamic pressure p_ℓ (39) and the shear stress $\mathbf{S}_\ell$ (37)-(46). In (48c), the covectors $\mathbf{e}_\ell^\beta$ are the columns of $\mathbf{F}_\ell^{-\top} = (\mathbf{e}_\ell^1, \mathbf{e}_\ell^2, \mathbf{e}_\ell^3)$, with $\mathbf{e}_\ell^\beta = (a_\ell^\beta, b_\ell^\beta, c_\ell^\beta)^\top$. Introducing $\mathbf{a}_\ell = (a_\ell^1, a_\ell^2, a_\ell^3)^\top$, $\mathbf{b}_\ell = (b_\ell^1, b_\ell^2, b_\ell^3)^\top$, $\mathbf{c}_\ell = (c_\ell^1, c_\ell^2, c_\ell^3)^\top$, then the unimodular Finger tensors in (37) writes:

$$\hat{\mathbf{G}}_\ell = \frac{1}{|\mathbf{G}_\ell|^{1/3}} \begin{pmatrix} \mathbf{a}_\ell.\mathbf{a}_\ell & \mathbf{a}_\ell.\mathbf{b}_\ell & \mathbf{a}_\ell.\mathbf{c}_\ell \\ \mathbf{a}_\ell.\mathbf{b}_\ell & \mathbf{b}_\ell.\mathbf{b}_\ell & \mathbf{b}_\ell.\mathbf{c}_\ell \\ \mathbf{a}_\ell.\mathbf{c}_\ell & \mathbf{b}_\ell.\mathbf{c}_\ell & \mathbf{c}_\ell.\mathbf{c}_\ell \end{pmatrix}, \qquad \ell = 0, \cdots, N. \tag{49}$$

In the right hand side of (48c), the relaxation tensors are deduced from (15), (29) and (30):

$$\mathbf{R}_0 = \mathbf{0}, \qquad \mathbf{R}_\ell = \frac{\theta_\ell}{2\mu_\ell} \left(\sigma_\ell - \frac{\lambda_\ell}{3\lambda_\ell + 2\mu_\ell} \mathrm{tr}(\sigma_\ell)\, \mathbf{I} \right), \qquad \ell = 1, \cdots, N. \tag{50}$$

Lastly, the equation (48d) is redundant with (48c). However, it is useful from a numerical point of view, to ensure that $J_\ell > 0$. Based on (19) and on (50), the scalars $\phi_\ell = J_\ell^{-1/2}\, \mathrm{tr}(\mathbf{R}_\ell)$ in (48d) are:

$$\phi_0 = 0, \qquad \phi_\ell = J_\ell^{-1/2} \frac{\theta_\ell}{3\lambda_\ell + 2\mu_\ell} \mathrm{tr}(\sigma_\ell), \qquad \ell = 1, \cdots, N. \tag{51}$$

Calibration. The parameters of the nonlinear Zener model are determined as follows:

1. the attenuation of the P- and S-wave is assumed to be known, for example via the quality factors of the compressional waves Q_p and the shear waves Q_s. An optimization procedure then provides the relaxation frequencies θ_ℓ and the weights $\kappa_\ell^{p,s}$;

2. the phase velocities of the compressional waves $c_p(0)$ and shear waves $c_s(0)$ provide the relaxed moduli π_r and μ_r, and then the unrelaxed moduli π_u and μ_u (23);

3. the Lamé coefficients (30)-(31) are deduced, and then the nonlinear parameter (45) involved in the hydrodynamic pressure;

4. the only free parameters are the χ_ℓ involved in the shear stress (46), with $-1 \leq \chi_\ell \leq 0.5$ to guarantee the hyperbolicity.

In the case of null dissipation, the weights are $\kappa_\ell^p = \kappa_\ell^s \equiv 0$ for $\ell = 1, \cdots, N$. It follows $\pi_u = \pi_r$, $\mu_u = \mu_r$ (23), $\lambda_\ell = \mu_\ell \equiv 0$ (30), and $\lambda_0 = \pi_r$, $\mu_0 = \mu_r$ (31). One has $\sigma_\ell = 0$ for $\ell = 1, \cdots, N$, and the system (48) recovers the hyperelastic model (4).

4 Numerical scheme

The inhomogenous system with source term (48) is solved numerically by a splitting method. A hyperbolic step solved by a Godunov-type scheme is followed by a relaxation step.

4.1 Hyperbolic step

This Section describes the resolution of the homogeneous part of (48) without source term. For the sake of simplicity, only 1D projections along x are described; the other projections are treated similarly. Removing ∂_y and ∂_z dependencies, one writes ($\ell = 0, \cdots, N$, $\beta = 1, 2, 3$):

$$
\begin{cases}
\dfrac{\partial \rho}{\partial t} + \dfrac{\partial (\rho u)}{\partial x} = 0, & \text{(52a)} \\
\dfrac{\partial}{\partial t} J_\ell^{-1/2} + \dfrac{\partial}{\partial x}(J_\ell^{-1/2} u) = 0, & \text{(52b)} \\
\dfrac{\partial (\rho u)}{\partial t} + \dfrac{\partial}{\partial x}\left(\rho u^2 - \sigma_{11}\right) = 0, & \text{(52c)} \\
\dfrac{\partial (\rho v)}{\partial t} + \dfrac{\partial}{\partial x}\left(\rho u v - \sigma_{12}\right) = 0, & \text{(52d)} \\
\dfrac{\partial (\rho w)}{\partial t} + \dfrac{\partial}{\partial x}\left(\rho u w - \sigma_{13}\right) = 0, & \text{(52e)} \\
\dfrac{\partial a_\ell^\beta}{\partial t} + \dfrac{\partial}{\partial x}\left(u a_\ell^\beta\right) + b_\ell^\beta \dfrac{\partial v}{\partial x} + c_\ell^\beta \dfrac{\partial w}{\partial x} = 0, & \text{(52f)} \\
\dfrac{\partial b_\ell^\beta}{\partial t} + u \dfrac{\partial b_\ell^\beta}{\partial x} = 0, & \text{(52g)} \\
\dfrac{\partial c_\ell^\beta}{\partial t} + u \dfrac{\partial c_\ell^\beta}{\partial x} = 0. & \text{(52h)}
\end{cases}
$$

This system is non conservative due to the governing equations of the geometrical variables (52f)-(52h). The resolution of (52) requires to determine the maximal sound velocities. In 3D, the computation of waves speed is very expensive due to the third degree characteristic polynoma, thus we will use an approximate expression of the maximum wave speed:

$$
c^2 = \zeta \sum_{\ell=0}^{N} \left(c_{h\ell}^2 + \frac{4}{3} \frac{\mu_\ell}{\rho_0} \right), \tag{53}
$$

where $c_{h\ell}$ are the hydrodynamic sound velocities (40), and $\zeta \geq 1$ is a security parameter [12, 24]. In the linear case, one recovers the sound speed of longitudinal waves when $\zeta = 1$.

We use the HLLC solver [30], because it preserves the positivity of the density and $J_\ell^{-1/2}$, and is able to deal with strong shock waves. Even if the equations of hyperelasticity contain 7 waves, we will use the solver containing only 3 waves: 2 waves having the most rapid characteristics (they correspond to longitudinal waves), and the contact characteristics. This simple solver is able to capture both longitudinal and transverse waves [14]. With such a solver, each wave is considered as a discontinuity and, consequently, jump relations are needed. The system being non-conservative, the usual Rankine-Hugoniot relation cannot be use, and each jump relation needs to be defined accross the waves, as done thereafter.

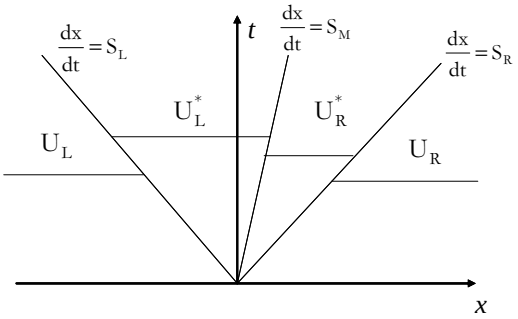

Figure 1: HLLC approximate solver. In the *star* region, two constant states are separated by a wave of speed S_M.

HLLC Riemann solver. We follow the lines of [11, 12, 25]. Let us consider a cell boundary separating a left state (L) and a right state (R), as sketched in Figure 1. The left and right facing wave speeds are obtained following Davis estimates [6]:

$$S_L = \min\left(u_L - c_L, u_R - c_R\right), \qquad S_R = \max\left(u_L + c_L, u_R + c_R\right), \tag{54}$$

where $c_{L,R}$ are the estimated maximal sound speeds (53). The speed of the contact discontinuity is estimated under the HLLC approximation:

$$S_M \equiv u^* = \frac{\left(\rho u^2 - \sigma_{11}\right)_L - \left(\rho u^2 - \sigma_{11}\right)_R - S_L\left(\rho u\right)_L + S_R\left(\rho u\right)_R}{\left(\rho u\right)_L - \left(\rho u\right)_R - \rho_L S_L + \rho_R S_R}. \tag{55}$$

Based on [30, 12], the conservative state variables in the star region are estimated by:

$$\left\{\begin{array}{l}
\rho^*_{L,R} = \rho_{L,R}\dfrac{S_{L,R} - u_{L,R}}{S_{L,R} - u^*}, \\
\left(J_\ell^{-1/2}\right)^*_{L,R} = \left(J_\ell^{-1/2}\right)_{L,R}\dfrac{S_{L,R} - u_{L,R}}{S_{L,R} - u^*}, \qquad \ell = 0, \cdots, N, \\
\sigma^*_{11} = \dfrac{\left(u_R - S_R\right)\rho_R\,\sigma_{11L} - \left(u_L - S_L\right)\rho_L\,\sigma_{11R} + \left(u_L - S_L\right)\rho_L\left(u_R - S_R\right)\rho_R\left(u_R - u_L\right)}{\left(u_R - S_R\right)\rho_R - \left(u_L - S_L\right)\rho_L}, \\
\sigma^*_{12} = \dfrac{\left(u_R - S_R\right)\rho_R\,\sigma_{12L} - \left(u_L - S_L\right)\rho_L\,\sigma_{12R} + \left(u_L - S_L\right)\rho_L\left(u_R - S_R\right)\rho_R\left(v_R - v_L\right)}{\left(u_R - S_R\right)\rho_R - \left(u_L - S_L\right)\rho_L}, \\
\sigma^*_{13} = \dfrac{\left(u_R - S_R\right)\rho_R\,\sigma_{13L} - \left(u_L - S_L\right)\rho_L\,\sigma_{13R} + \left(u_L - S_L\right)\rho_L\left(u_R - S_R\right)\rho_R\left(w_R - w_L\right)}{\left(u_R - S_R\right)\rho_R - \left(u_L - S_L\right)\rho_L}, \\
v^* = \dfrac{\left(\rho u v - \sigma_{12}\right)_L - \left(\rho u v - \sigma_{12}\right)_R - S_L\left(\rho v\right)_L + S_R\left(\rho v\right)_R}{\left(\rho v\right)_L - \left(\rho v\right)_R - \rho_L S_L + \rho_R S_R}, \\
w^* = \dfrac{\left(\rho u w - \sigma_{13}\right)_L - \left(\rho u w - \sigma_{13}\right)_R - S_L\left(\rho w\right)_L + S_R\left(\rho w\right)_R}{\left(\rho w\right)_L - \left(\rho w\right)_R - \rho_L S_L + \rho_R S_R}.
\end{array}\right. \tag{56}$$

In the case of a fluid-solid interface [25], the velocities v^* and w^* can be discontinuous in the region *star*, so that one must define $v^*_{L,R}$ and $w^*_{L,R}$. In the case of a pure solid considered here, these fields are on the contrary constant in the whole region *star*. Then, the geometric variables

are ($\ell = 0, \cdots, N$, $\beta = 1, 2, 3$):

$$\begin{cases} \left(a_\ell^\beta\right)^*_{L,R} = \dfrac{\left(a_\ell^\beta\right)_{L,R}(u_{L,R} - S_{L,R}) + \left(b_\ell^\beta\right)_{L,R}(v_{L,R} - v^*) + \left(c_\ell^\beta\right)_{L,R}(w_{L,R} - w^*)}{u^* - S_{L,R}}, \\ \left(b_\ell^\beta\right)^*_{L,R} = \left(b_\ell^\beta\right)_{L,R}, \\ \left(c_\ell^\beta\right)^*_{L,R} = \left(c_\ell^\beta\right)_{L,R}. \end{cases} \tag{57}$$

With the jump relation presented previously, it is now possible to determine the flux at each cells boundaries. From now on, we will denote with the star superscript * the sampled flux obtained:

$$A^\star = \begin{cases} A_L & \text{if} \quad S_L \geq 0, \\ A_R & \text{if} \quad S_R \leq 0, \\ A_R^\star & \text{if} \quad S_M \leq 0 \leq S_R, \\ A_L^\star & \text{if} \quad S_M \geq 0 \geq S_L. \end{cases} \tag{58}$$

With these definition, we can now derive the numerical scheme

Godunov type scheme. The system (52) contains conservative and non-conservative equations, which are solved successively. The conservative part of (52) reads as a $5 + N$ system

$$\frac{\partial \mathbf{U}}{\partial t} + \frac{\partial \mathbf{f}}{\partial x} = \mathbf{0}, \tag{59}$$

with the vector of conserved variables

$$\mathbf{U} = \left(\rho,\, J_\ell^{-1/2},\, \rho u,\, \rho v,\, \rho w\right)^\top, \qquad \ell = 0, \cdots, N, \tag{60}$$

and the flux

$$\mathbf{f} = \left(\rho u,\, J_\ell^{-1/2} u,\, \rho u^2 - \sigma_{11},\, \rho uv - \sigma_{12},\, \rho uw - \sigma_{13}\right)^\top. \tag{61}$$

Given a time step Δt and and a mesh size Δx, the usual Godunov scheme is applied [20]:

$$\mathbf{U}_i^{n+1} = \mathbf{U}_i^n - \frac{\Delta t}{\Delta x}\left(\mathbf{f}^*_{i+1/2} - \mathbf{f}^*_{i-1/2}\right), \tag{62}$$

where $\mathbf{U}_i^n \approx \mathbf{U}(x_i = i\Delta x, t_n = t_{n-1} + \Delta t)$. The numerical flux $\mathbf{f}^*_{i+1/2} = \mathbf{f}^*(\mathbf{U}_i^n, \mathbf{U}_{i+1}^n)$ is given by the *star* variables: $\mathbf{f}^*(\mathbf{U}_L, \mathbf{U}_R) = \mathbf{f}(\mathbf{U}^*)$. In practice, instead of calculating the density via (60)-(62), we use the expression $\rho = \rho_0 J_0^{-1/2}$. This saves an array of data.

The system for the non-conservative part of (52) reads as a $9 \times (N + 1)$ system:

$$\frac{\partial \mathbf{W}_\ell^\beta}{\partial t} + \frac{\partial \mathbf{g}_\ell^\beta}{\partial x} + \mathbf{k}_{u,\ell}^\beta \frac{\partial u}{\partial x} + \mathbf{k}_{v,\ell}^\beta \frac{\partial v}{\partial x} + \mathbf{k}_{w,\ell}^\beta \frac{\partial w}{\partial x} = \mathbf{0}, \tag{63}$$

with the vector of non-conserved variables

$$\mathbf{W}_\ell^\beta = \left(a_\ell^\beta,\, b_\ell^\beta,\, c_\ell^\beta\right)^\top, \qquad \ell = 0, \cdots, N, \qquad \beta = 1, 2, 3, \tag{64}$$

and the fluxes

$$\mathbf{g}_\ell^\beta = \left(ua_\ell^\beta,\, ub_\ell^\beta,\, uc_\ell^\beta\right)^\top, \quad \mathbf{k}_{u,\ell}^\beta = \left(0,\, -b_\ell^\beta,\, -c_\ell^\beta\right)^\top, \quad \mathbf{k}_{v,\ell}^\beta = \left(b_\ell^\beta,\, 0,\, 0\right)^\top, \quad \mathbf{k}_{w,\ell}^\beta = \left(c_\ell^\beta,\, 0,\, 0\right)^\top. \tag{65}$$

The non-conservative equations are solved by the scheme:

$$\begin{aligned}\left(\mathbf{W}_\ell^\beta\right)_i^{n+1} &= \left(\mathbf{W}_\ell^\beta\right)_i^n - \frac{\Delta t}{\Delta x}\left[\left(\mathbf{g}_\ell^\beta\right)_{i+1/2}^* - \left(\mathbf{g}_\ell^\beta\right)_{i-1/2}^* + \left(\mathbf{k}_{u,\ell}^\beta\right)_i^n\left(u_{i+1/2}^* - u_{i-1/2}^*\right)\right. \\ &+ \left.\left(\mathbf{k}_{v,\ell}^\beta\right)_i^n\left(v_{i+1/2}^* - v_{i-1/2}^*\right) + \left(\mathbf{k}_{w,\ell}^\beta\right)_i^n\left(w_{i+1/2}^* - w_{i-1/2}^*\right)\right].\end{aligned} \tag{66}$$

The numerical flux $\left(\mathbf{g}_\ell^\beta\right)_{i+1/2}^* = \left(\mathbf{g}_\ell^\beta\right)^*\left(\left(\mathbf{W}_\ell^\beta\right)_i^n, \left(\mathbf{W}_\ell^\beta\right)_{i+1}^n\right)$ is given by the *star* variables: $\left(\mathbf{g}_\ell^\beta\right)^*(\mathbf{W}_L, \mathbf{W}_R) = \mathbf{f}_2(\mathbf{W}^*)$. In (66), $u_{i\pm1/2}^*$ are the normal velocity components at the cell boundaries, $v_{i-1/2}^*$ and $w_{i+1/2}^*$ are the corresponding tangential velocity components.

The conservative and non-conservative parts of the Godunov scheme are solved simultaneously. As already pointed out, only 1D fluxes are written (62) and (66). For multidimensional problems, these fluxes must be completed by the y and z dependencies. The CFL condition of stability of this method is

$$\mathrm{CFL} = \max(c)\frac{\Delta t}{\Delta x} \leq 0.5, \tag{67}$$

where $\max(c)$ denotes the maximal value of (53) over the computational domain.

4.2 Relaxation step

In the final system (48), the only equations that are changing during the relaxation step are

$$\begin{cases} \dfrac{\partial \mathbf{e}_\ell^\beta}{\partial t} = \dfrac{\theta_\ell}{2\mu_\ell}\left(\sigma_\ell - \dfrac{\lambda_\ell}{3\lambda_\ell + 2\mu_\ell}\operatorname{tr}(\sigma_\ell)\,\mathbf{I}\right).\mathbf{e}_\ell^\beta, & \ell = 1,\cdots,N, \quad \beta = 1,2,3, \qquad (68a) \\ \dfrac{\partial}{\partial t}J_\ell^{-1/2} = \dfrac{\theta_\ell}{3\lambda_\ell + 2\mu_\ell}\operatorname{tr}(\sigma_\ell)\,J_\ell^{-1/2}, & \ell = 1,\cdots,N. \qquad (68b) \end{cases}$$

This system of $10 \times N$ ordinary differential equations could be solved by any numerical integrator. However, a naive resolution of (68) would not ensure $|\mathbf{F}_\ell| > 0$, which is essential when computing the energy (37).

An alternative approach is followed here to ensure the positivity of $|\mathbf{F}_\ell|$ and J_ℓ. Assuming that σ_ℓ is constant during the relaxation step, then (68) can be integrated exactly:

$$\begin{cases} \left(\mathbf{e}_\ell^\beta\right)^{n+1} = \exp\left(\dfrac{\theta_\ell \Delta t}{2\mu_\ell}\left(\sigma_\ell - \dfrac{\lambda_\ell}{3\lambda_\ell + 2\mu_\ell}\operatorname{tr}(\sigma_\ell)\,\mathbf{I}\right)\right).\left(\mathbf{e}_\ell^\beta\right)^n, \ \ell = 1,\cdots,N, \ \beta = 1,2,3 \qquad (69a) \\ \left(J_\ell^{-1/2}\right)^{n+1} = \exp\left(\dfrac{\theta_\ell \Delta t}{3\lambda_\ell + 2\mu_\ell}\operatorname{tr}(\sigma_\ell)\right)\left(J_\ell^{-1/2}\right)^n, \quad \ell = 1,\cdots,N. \qquad (69b) \end{cases}$$

The computation of the matrix exponential (69a) is done by a (6, 6) Padé approximation of the "scaling and squaring method" [23]. The equation on $J_\ell^{-1/2}$ is used only in the hydrodynamic pressure (39). Doing so provides an easy mean to guarantee that isochoric transformations do not modify the hydrodynamic energy (38).

5 Numerical examples

5.1 Shear Riemann problem

A domain $[0, 1]$ of length $L = 1$ m is discretized on 2000 points. The medium is hyperelastic, with reference density $\rho_0 = 1200$ kg.m^{-3}, compressional wave velocity $c_p(0) = 2800$ m/s, and shear

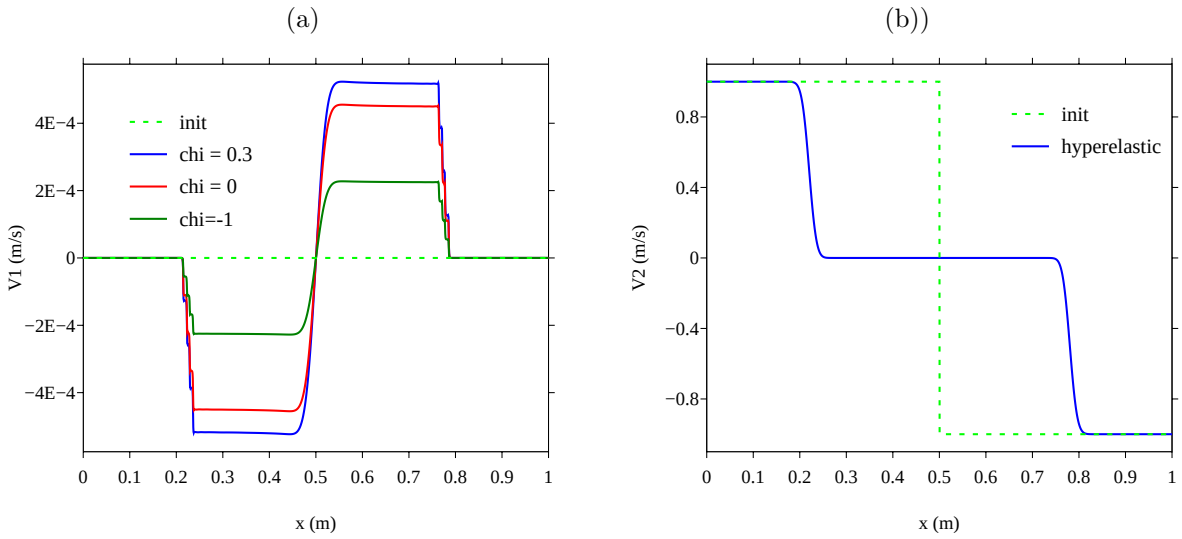

Figure 2: Shear Riemann problem in hyperelasticity. Initially a discontinuous tangential velocity is imposed (dashed line). Various values of the nonlinear parameter χ are considered, leading to different amplitudes of v_1.

wave velocity $c_s(0) = 1400$ m/s. The fields are initially zero, excep the tangential velocity which is discontinuous at $x_0 = 0.5$ m: $v_2 = 1$ m/s for $x < x_0$, and $v_2 = -1$ m/s for $x > x_0$.

Figure 2-left represents the longitudinal and tangential velocities at $t = 2\,10^{-4}$ s. In linear regime, v_1 would remain identically zero. On the contrary, one observes here that longitudinal waves are generated, which is the signature of a nonlinear coupling. The amplitude of these longitudinal waves depends on the nonlinear parameter $\chi_0 \equiv \chi$. The tangential component of the velocity v_2 has right-going and left-going shock waves, and is independent of χ for the amplitude considered here. From now on, we will consider $\chi_\ell = 0$.

5.2 Impact Riemann problem

	θ_ℓ	κ_ℓ	θ_ℓ	κ_ℓ
$\ell = 1$	1652	0.386	1372	0.0874
$\ell = 2$	14153	0.399	11885	0.0723
$\ell = 3$	123603	0.726	103368	0.1025

Table 1: Optimized parameters of viscoelasticity for the impact Riemann problem. The range of optimization is $[1.12\,10^3, 1.12\,10^5]$ Hz. Left part: $Q = 5$; right part: $Q = 20$.

Given the same parameters as before, we now consider an impact with a longitudinal velocity discontinuity: $v_1 = +1$ m/s for $x < x_0$, and $v_1 = -1$ m/s for $x > x_0$. The dissipation is accounted for by $N = 3$ relaxation mechanisms, with the same quality factor for compressional and longitudinal waves: $Q_p = Q_s \equiv Q$. The value $Q = 20$ corresponds to low dissipation, while $Q = 5$ corresponds to high dissipation. The Zener model parameters are optimised over a frequency band $[f_{\min}, f_{\max}]$, with $f_{\min} = f_c/10$ and $f_{\max} = 10 \times f_c$ [3]. The central frequency is

chosen so that $f_c = c_p/\lambda$, where λ is a characteristic length. Here $\lambda = L/4 = 0.25$ is chosen, so that $f_c = 11.2$ kHz. The optimized parameters are given in Table 1.

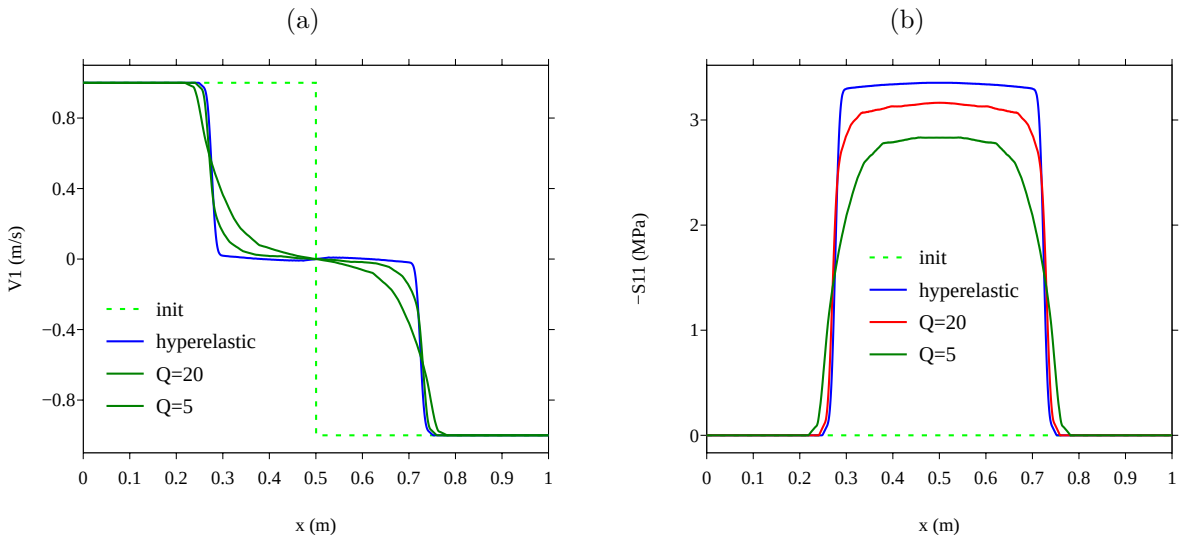

Figure 3: Impact Riemann problem. Initially a discontinuous longitudinal velocity is imposed (dashed line). Various values of attenuation are considered: null (hyperelasticity), weak ($Q = 20$) and large ($Q = 5$). Left: v_1; right: $-\sigma_{11}$.

Figure 3 shows the longitudinal velocity v_1 and the total stress component $-\sigma_{11}$ at $t = 8\,10^{-5}$ s. In the absence of dissipation (hyperelastic medium), shock waves propagate in both directions. As the attenuation increases, the sharp fronts are smoother, and the amplitude of σ_{11} decreases.

5.3 Compressive source point in 1D

We consider a 1D problem with a source point at $x_s = 0.5$ m, which emits a compressive sine wave from $t = 0$. In (48b), the source term is then $\mathbf{s}(x,t) = A \sin(\omega_c t)\, H(t)\, \delta(x - x_s)\, (1,0)^\top$ with $\omega_c = 2\pi\, f_c$, and an amplitude $A = 2\,10^7$. The central frequency is $f_c = 20$ kHz; the parameters of the Zener model ($N = 3$ relaxation mechanisms) are optimised accordingly. The optimized parameters are given in the left part of Table 2.

	θ_ℓ	κ_ℓ	θ_ℓ	κ_ℓ
$\ell = 1$	2950	0.386	1475	0.386
$\ell = 2$	25271	0.399	12637	0.399
$\ell = 3$	220716	0.726	110359	0.726

Table 2: Optimized parameters of viscoelasticity for the source point problems. The quality factor is $Q = 5$. Left part: 1D case, with optimization range $[2\,10^3,\ 2\,10^5]$ Hz. Right part: 2D case, with optimization range $[10^3,\ 10^5]$ Hz.

Figure 4 displays a snapshot of v_1 at $t = 1.5\,10^{-4}$ s. In the hyperelastic case, we observe the asymmetry of the waves with respect to the source point. Another signature of nonlinearities is the appearance of shocks. In the case of the Zener model (right), the fields are still asymmetric.

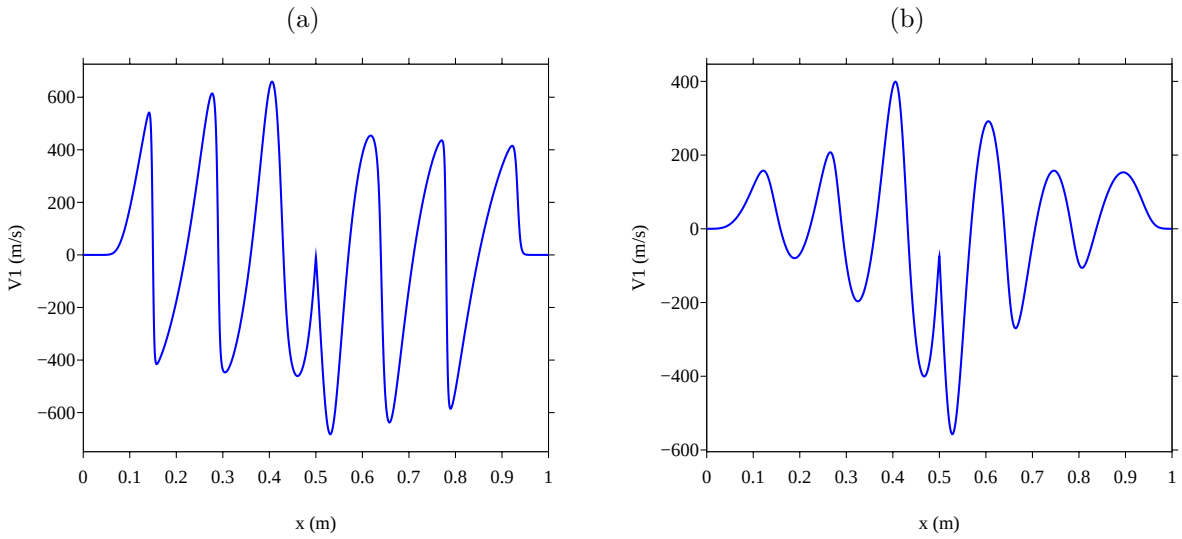

Figure 4: Snapshot of v_1 and v_2 at $t = 1.5\,10^{-4}$ s. A monochromatic source at $x_s = 0.5$ emits compressive monochromatic waves with an amplitude $A = 2\,10^7$ and a central frequency $f_c = 20$ kHz. Right: viscoelastic medium, with $Q = 5$ ($N = 3$ relaxation mechanisms).

However, the dissipation is sufficient to smooth the sharp fronts and to prevent the occurrence of shocks.

5.4 Shear source point in 1D

We consider a 1D problem with a point source at $x_s = 0.5$ m, which emits a shear sine wave from $t = 0$. In (48b), the source term is then $\mathbf{s}(x,t) = A \sin(\omega_c t)\, H(t)\, \delta(x - x_s)\, (0,1)^\top$. All the parameters are the same as in the previous test with compressive source. In particular, the amplitude of the forcing is $A = 2\,10^7$, and the central frequency is $f_c = 20$ kHz.

Figure 5 displays a snapshot of v_1 and v_2 at $t = 1.5\,10^{-4}$ s. In linear regime, no compressional wave would be emitted. On the contrary, one observes clearly in (a-c) a v_1 component, whose amplitude is roughly 20% of the amplitude of v_2 (b-d). The latter shear wave propagates slower. For both components, the effect of viscoelasticity is clearly seen through the damping of waves..

5.5 Source point in 2D

As a last example, we consider a 2D domain $[-0.5, 0.5]^2$, discretized on 300^2 points in space. The parameters of the viscoelastic medium are the same as before, with $Q_p = Q_s = 5$. The optimized parameters are given in the right part of Table 2. A source is placed in the center of the domain. The forcing (48b) is $\mathbf{s}(\mathbf{x},t) = A\, r(\mathbf{x})\, g(t)\, (1,0)^\top$. The spatial distribution r is a Gaussian of radius 0.08 m and standard deviation 0.04 m. By regularising the Dirac in this way, singularities in the solution and spurious oscillations at the source are avoided. The time evolution $g(t)$ is a Ricker [3], of central frequency $f_c = 10$ kHz. Two forcing amplitudes are considered: $A = 10^7$ (low amplitude) and $A = 10^9$ (large amplitude). A receiver in $(x_r = 0.05, y_r = 0.05)$ records the field at each iteration. It is denoted by a yellow cross on the carts of Figure 6.

The maps in Figure 6 show v_1 and v_2 at $t = 1.9\,10^{-4}$ s. At low amplitude (a-b), we observe the

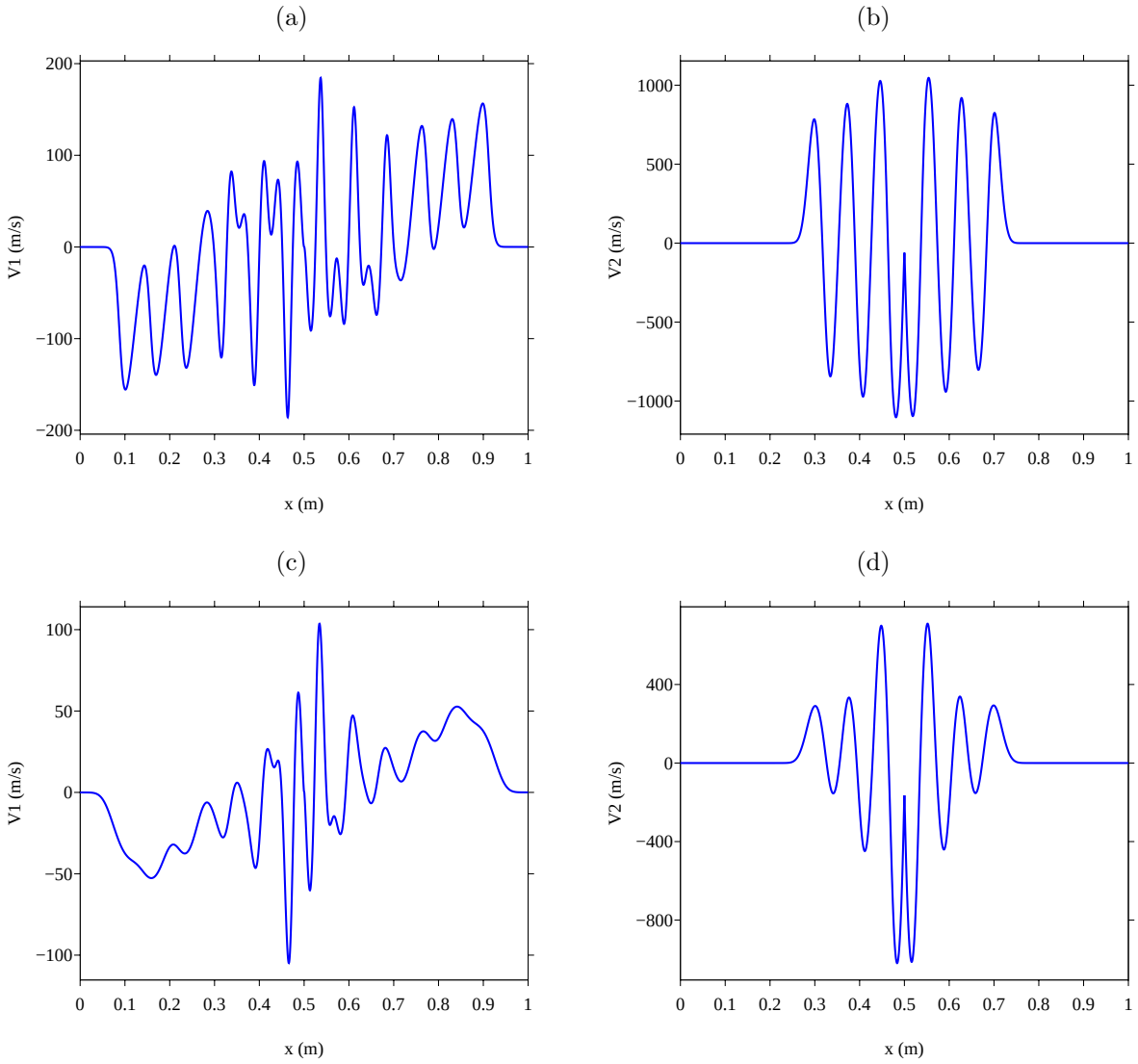

Figure 5: Snapshot of v_1 (left row) and v_2 (right row) at $t = 1.5\,10^{-4}$ s. A monochromatic source at $x_s = 0.5$ emits shear monochromatic waves with an amplitude $A = 2\,10^7$ and a central frequency $f_c = 20$ kHz. Top (a-b): hyperelastic medium. Bottom (c-d): viscoelastic medium, with $Q = 5$ ($N = 3$ relaxation mechanisms).

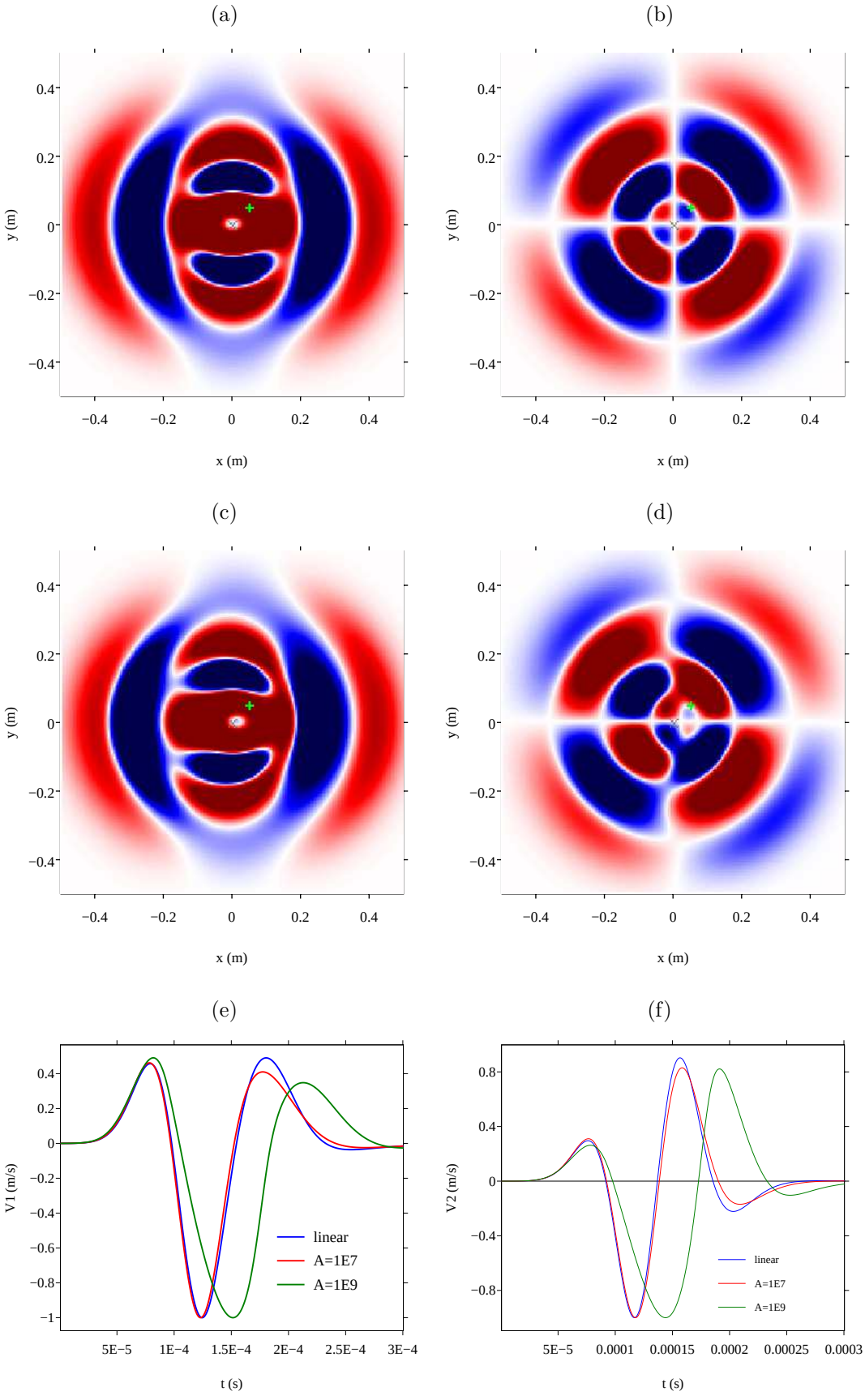

Figure 6: Two dimensional fields emitted by a source point (denoted by a yellow cross). The carts represent v_1 (left) and v_2 at $t = 1.9\,10^{-3}$ s, for low amplitudes (a-b) and large amplitudes (c-d). The curves display the time evolution of the normalizedv_1 (e) and v_2 (f) computed by the linear Zener model and by the nonlinear Zener model, for two amplitudes. One can note that the figure becomes non symmetric when amplitude becomes larger.

expected properties of symmetry of v_1 with respect to $x = 0$, and of central symmetry of v_2. We also observe on v_2 the separation into compressional and shear waves. At high amplitudes (c-d), the symmetry properties are lost, which is a signature of non-linear effects.

Figure 6 shows the time evolution of v_1 and v_2 measured at the receiver, up to $t = 3\,10^{-4}$ s. The normalized signals obtained with the linear Zener model [21] and the nonlinear model are superimposed. At low amplitude ($A = 10^7$), we note the good agreement between the linear model and the nonlinear Zener model: the nonlinear effects are moderate. At large amplitude ($A = 10^9$), the nonlinear effects distort the signals significantly.

6 Conclusion

We have proposed a nonlinear viscoelasticity model well adapted to the dynamic regime. This model degenerates to two classical limiting cases: (i) hypelasticity when dissipation cancels; (ii) to the linear Zener model in small deformations. The proposed model is dissipative and unconditionally hyperbolic, leading to explicit and reliable numerical schemes. Here a robust first-order Godunov scheme is used, but more sophisticated schemes can obviously be implemented to reduce the numerical diffusion [4].

A similar approach can be followed to describe a richer phenomenology. One thinks in particular of thermo-elastic solids, or of the study of waves in yield stresses fluids [26].

References

[1] H. Berjamin, N. Favrie, B. Lombard, G. Chiavassa, *Nonlinear waves in solids with slow dynamics: an internal-variable model*, Proceedings Royal Society London A 473 (2017), 20170024.

[2] H. Berjamin, B. Lombard, G. Chiavassa, N. Favrie, *Modeling longitudinal wave propagation in nonlinear viscoelastic solids with softening*, International Journal of Solids and Structures 141-142 (2018), 35-44.

[3] E. Blanc, D. Komatitsch, E. Chaljub, B. Lombard, Z. Xie, *Highly-accurate stability-preserving optimization of the Zener viscoelastic model, with application to wave propagation in the presence of attenuation*, Geophysical Journal International, 205 (2016), 427-439.

[4] S. Busto Ulloa, S. Chiocchetti, M. Dumbser, E. Gaburro, I. Peshkov, *High Order ADER Schemes for Continuum Mechanics*, Frontiers in Physics, 8 (2020)

[5] J.M. Carcione, *Wave Fields in Real Media: Wave Propagation in Anisotropic, Anelastic, Porous and Electromagnetic Media*, Pergamon (2007).

[6] S.F. Davis, *Simplified second-order Godunov-type methods*, SIAM J. Sci. Stat. Comput., 9 (1988), 445-473.

[7] N. Delépine, L. Lenti, G. Bonnet, J.F. Semblat, *Non-linear viscoelastic wave propagation: an extension of nearly constant attenuation models*, Journal of Engineering Mechanics, 135-11 (2009), 1305–1314.

[8] D. Espíndola, S. Lee, G. Pinton, *Shear shock waves observed in the brain*, Physical Review Applied, 8-4 (2017), 044024.

[9] N. Favrie, S. Gavrilyuk, *Mathematical and numerical model for nonlinear viscoplasticity*, Philosophical Transactions of the Royal Society of London A: Mathematical, Physical and Engineering Sciences, 369 (2011), 2864-2880.

[10] N. Favrie, S. Gavrilyuk, *Dynamics of shock waves in elastic-plastic solids*, ESAIM: Proceedings, 33 (2011), 50-6.

[11] N. Favrie, S. Gavrilyuk, *Diffuse interface model for compressible fluid – Compressible elastic–plastic solid interaction.* Journal of Computational Physics, 231 (2012), 2695-2723.

[12] N. Favrie, S. Gavrilyuk, S. Ndanou, *A thermodynamically compatible splitting procedure in hyperelasticity*, Journal of Computational Physics, 270 (2014), 300-324.

[13] N. Favrie, B. Lombard, C. Payan, *Fast and slow dynamics in a nonlinear elastic bar excited by longitudinal vibrations*, Wave Motion, 56 (2015), 221-238.

[14] S. Gavrilyuk, N. Favrie, R. Saurel, *Modelling wave dynamics of compressible elastic materials*, Journal of Computational Physics, 227 (2008), 2941–2969.

[15] S. Gavrilyuk, S. Ndanou, S. Hank, *An example of a one-parameter family of rank-one convex stored energies for isotropic compressible solids*, Journal of Elasticity, 124 (2016), 133-141.

[16] S.K. Godunov, E.I. Romenskii, *Elements of Continuum Mechanics and Conservation Laws*, Kluwer Academic Plenum Publishers, NY (2003).

[17] G. A. Holzapfel, *Nonlinear Solid Mechanics: A Continuum Approach for Engineering*, John Wiley & Sons Ltd., 2000.

[18] P. Le Tallec, C. Rahier, A. Kaiss, *Three-dimensional incompressible viscoelasticity in large strains: formulation and numerical approximation*, Computer Methods in Applied Mechanics and Engineering, 109 (1993), 233-258.

[19] J. Lemaitre, J.-L. Chaboche, A. Benallal, R. Desmorat, *Mécanique des Matériaux Solides*, 3rd Edition, Dunod, 2009.

[20] R.J. LeVeque, *Finite Volume Methods for Hyperbolic Problems*, Cambridge University Press (2002).

[21] B. Lombard, J. Piraux, *Numerical modeling of transient two-dimensional viscoelastic waves*, Journal of Computational Physics, 230 (2011), 6099-6114.

[22] R. Martin, L. Bodet, V. Tournat, F. Reijiba, *Seismic wave propagation in nonlinear viscoelastic media using the auxiliary differential equation method*, Geophysical Journal International, 216 (2019), 453-469.

[23] C.B. Moller, C.F. Loan, *Nineteen dubious ways to compute the exponential of a matrix, twenty-five years later*, SIAM Review, 45 (2003), 3–49.

[24] S. Ndanou, N. Favrie, S. Gavrilyuk, *Criterion of hyperbolicity in hyperelasticity in the case of the stored energy in separable form*, Journal of Elasticity, 115 (2014), 1-25.

[25] S. Ndanou, N. Favrie, S. Gavrilyuk, *Multi-solid and multi-fluid diffuse interface model: applications to dynamic fracture and fragmentation*, Journal of Computational Physics, 295 (2015), 523-555.

[26] A. Perelomova, *Propagation of acoustic pulses in some fluids with yield stress*, Canadian Journal of Physics, 89 (2011), 219-224.

[27] S. Reese, S. Govindjee, *A theory of finite viscoelasticity and numerical aspects*, International Journal of Solids and Structures, 35 (1998), 3455-3482.

[28] J.O.A. Robertsson, J.O. Blanch, W.W. Symes, *Viscoelastic finite-difference modeling*, Geophysics, 59-9 (1994), 1444-1456.

[29] B.B. Tripathi, D. Espíndola, G.F. Pinton, *Modeling and simulations of two dimensional propagation of shear shock waves in relaxing soft solids*, Journal of Computational Physics 395 (2019), 205-222.

[30] E. F. Toro, *Riemann Solvers and Numerical Methods for Fluid Dynamics. A Practical Introduction*, Springer-Verlag (1999).

[31] V. Tournat, V. Gusev, *Acoustics of unconsolidated model granular media: an overview of recent results and several open problems*, Acta Acustica United Acustica, 96 (2010), 208–224.

[32] A. Wineman, *Nonlinear viscoelastic solids—a review*, Mathematics and Mechanics of Solids, 14-3 (2009), 300–366.